Journal of Vibration Engineering & Technologies (2018) 6:155–161
https://doi.org/10.1007/s42417-018-0020-9

ORIGINAL PAPER

Effect of Piezoelectric Patch Size and Material on Active Vibration Control of Wind Turbine Blades

Wael G. Abdelrahman[1] · Ahmed Z. Al-Garni[1] · Sherif I. Abdelmaksoud[1] · Ayman Abdallah[1]

Received: 22 June 2015 / Revised: 21 August 2015 / Accepted: 27 January 2016 / Published online: 23 June 2018

Abstract

Purpose The purpose of this study is to investigate the effect of piezoelectric actuator patch size and material on the active vibration control of wind turbine blades.

Methods This work builds on a recently developed numerical technique to reduce vibrations in wind turbine blades. Control action is achieved by bonding a piezoelectric actuator on the upper surface of the blade and a similar piezoelectric sensor on the blade's lower surface. An approximate analytical method is used to solve the governing equations to obtain dynamic characteristics of the smart blade. Modal coordinates are used to obtain the model in state space form, then a linear quadratic regulator controller is used to provide active control.

Results The system is solved for different piezoelectric patch sizes and materials. Results show that increasing the values of piezoelectric stress/charge (e_{31}) increases both the maximum blade displacement and required actuation force.

Conclusions Using piezoelectric patches with reduced (e_{31}) can effectively decrease blade vibrations.

Keywords Active vibration control · Wind turbine blade · Piezoelectric patches · Smart materials · Approximate analytical methods

Introduction

Wind has long been one of the most important, sustainable, and economical sources of renewable energy. Because no fossil fuel is used in them, wind turbine power stations provide a competitive supply of electrical energy while occupying less space than conventional power stations. According to the International Renewable Energy Agency, global wind energy capacity increased 130% between 2009 and 2014. In many countries, wind energy can play a major role toward reducing demand of fossil fuel, especially in remote locations with abundant wind. Wind turbine blades are the main wind turbine components that introduce vibrations into the system. These vibrations can cause catastrophic damage due to structural fatigue and progressive failure of the light weight structure, resulting in unscheduled maintenance, reduced efficiency, and shortened lifetime.

To improve reliability of such light-weight structures, several techniques were conducted experimentally and numerically either to limit or to change the vibration response of such systems. With recent developments in sensor/actuator technologies and in smart materials, especially piezoelectric materials, active vibration control has been utilized for vibration suppression. The dynamic characteristics of the structure are needed before designing an active controller. In their work, Achawakorn and Jearsiripongkul [1] determined the vibration properties of both uniform and a nonuniform cantilever beams using an approximate analytical method, whereas Bazoune and Khulief [2] developed a finite beam element for vibration characteristics of a tapered rotating Timoshenko beam. The work was specified to turbine blades in subsequent research work. Gireesh Kumar and Sjatha [3] studied both the free and forced response of these blades using a combination of measurement results and the finite-element method. A considerable body of research

✉ Ahmed Z. Al-Garni
algarni@kfupm.edu.sa

Wael G. Abdelrahman
wgamal@kfupm.edu.sa

Sherif I. Abdelmaksoud
sherifibrahim@kfupm.edu.sa

Ayman Abdallah
aymanma@kfupm.edu.sa

[1] King Fahd University Of Petroleum and Minerals, Dhahran 31261, Saudi Arabia

was directed to investigate vibration suppression using piezoelectric materials. Crawley and De Luis [4] showed introduced, analytically and experimentally, piezoelectric materials as actuators and sensors embedded within smart beams. Han et al. [5] used Ritz solution of the governing equation and the classical laminated plate theory to model the active vibration control of smart composite cantilever beams and plates.

Several types of controllers were considered in the literature for active vibration suppression. The work of Zhang et al. [6, 7] studied the effect of linear quadratic regulator (LQR), LQG, and robust control H_∞ for vibration reduction, whereas the studies of Manjunath and Bandyopadhyay [8, 9] considered the design of a periodic output feedback (POF). More recently, artificial neural network (ANN) simulation and evolutionary algorithms were considered for modeling, analysis, and predicting structural response. They can be used for determining both the optimal size and location of the sensors and actuators on the structure, and for designing the optimal control. For example, Roy and Chakraborty [10] combined a LQR with a genetic algorithm (GA) to optimize controller parameters. Kumar and Chhabra [11] used ANN to better design a LQR. Zoric et al. [12] used both fuzzy optimization and particle swarm optimization (PSO) algorithm to develop optimal control parameters. Recently, Abdelmaksoud et al. [13] suggested a model for active vibration control using PD and LQR controllers.

In this study, active vibration control method is conducted numerically for vibration suppression of a wind turbine blade model, using a piezoelectric sensor and actuator. APD controller and LQR optimal control are designed to provide the control input to the actuator. After that, the effects of piezoelectric size and piezoelectric material properties on vibration response are investigated.

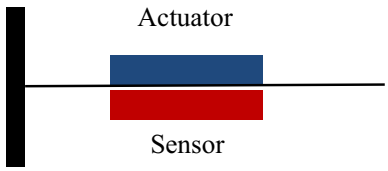

Fig. 1 Model of smart wind turbine blade with a single piezoelectric sensor and actuator

Mathematical Model

The mathematical model is presented in detail in [13]. It is summarized here for clarity. The smart wind turbine blade is modeled as a tapered cantilever beam with one sensor bonded to the middle of the lower surface, and one actuator bonded to the middle of the upper surface, as shown in Fig. 1.

Several types of airfoils have been used for blade cross section. These include the symmetric NACA0012 airfoil, and cambered NACA 4415 and NACA 63(2)-215 airfoils [14]. In this study, a NACA 0012 airfoil with a thickness ratio of 12% is used [15], as shown in Fig. 2.

The formula of thickness distribution is required to obtain the cross section and second moment of area. For this family of airfoils, NACA 4-digit series, the symmetrical thickness distribution is given by [13]:

$$y = \frac{Tc}{0.2}\left[a_1\sqrt{\frac{z}{c}} + a_2\frac{z}{c} + a_3\left(\frac{z}{c}\right)^2 + a_4\left(\frac{z}{c}\right)^3 + a_5\left(\frac{z}{c}\right)^4\right], \tag{1}$$

where $a_1 = 0.2969$, $a_2 = -0.126$, $a_3 = -0.3516$, $a_4 = 0.2843$, and $a_5 = -0.1015$

Blade cross section area can be simply obtained by integration. Second moment of area of the blade cross section is expressed as:

$$I_{xx} = \int y_t^2 \mathrm{d}A = \int_0^c \int_0^y y_t^2 \mathrm{d}y\mathrm{d}z. \tag{2}$$

Throughout this study, the blade is assumed to be made of a commonly used Aluminum alloy, namely Al-6061. This material has and elastic modulus $E = 69$ GPa and density $= 2705$ kg/m^3. The damping constants, and , are selected to be 0.001 and 0.0001, respectively. The length of the wind turbine blade model used is 200 cm. The root and tip chord of the wind turbine blade model are 25 and

Fig. 2 Wind turbine blade NACA 0012 airfoil section

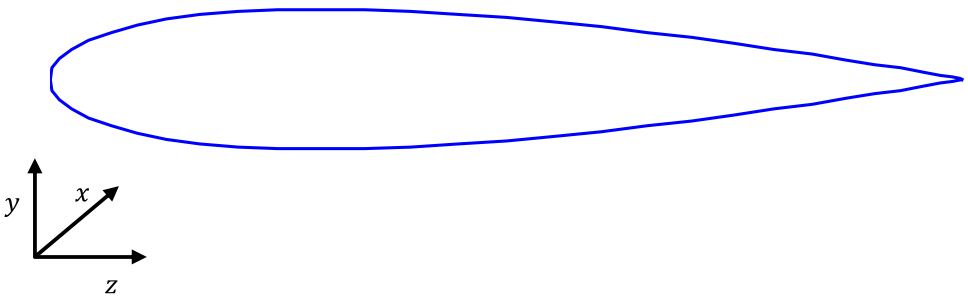

Table 1 Material properties of piezoelectric sensor/actuator (PZT)

Properties	Units	Sensor	Actuator
L (length)	cm	11.3	11.3
W (width)	cm	10.7	10.7
t (thickness)	mm	0.5	0.5
d_{31} (piezo strain constant)	m/V	-125×10^{-12}	-125×10^{-12}
g_{31} (voltage constant)	mV/N	-1.16×10^{-2}	-1.16×10^{-2}
e_{31} (piezoelectric stress/charge)	C/m^2	−10.62	−10.62
K_{31} (coupling coefficient)	–	0.35	0.35
E (Young's modulus)	GPa	63	63
ρ (density)	kg/m^3	7600	7600

10 cm, respectively. The thickness to chord ratio is 12%. Material properties of the basic piezoelectric (PZT) sensor/actuator patches used are given in Table 1.

The partial differential equation of motion for Euler–Bernoulli tapered beam where the transverse deflection $w(x,\ t)$ and for free vibration can be expressed as

$$\rho A(x)\frac{\partial^2\omega(x,t)}{\partial t^2}+\frac{\partial^2}{\partial x^2}\left[EI(x)\frac{\partial^2\omega(x,t)}{\partial x^2}\right]=0, \tag{3}$$

where E represents Young's modulus, whereas $A(x)$ is the cross section area and $I(x)$ represent the moment of inertia of the tapered beam, respectively. is the mass density.

The displacement solution $w(x,t)$ can be expanded in the form

$$w(x,t)=\sum_{i=1}^{n}\emptyset_i(x)\eta_i(t), \tag{4}$$

where η_1, η_2,…,η_n are the generalized coordinates, and $\emptyset_1(x)$, $\emptyset_1(x)$,…, $\emptyset_n(x)$ are the shape functions that depend on the boundary condition. Several families of shape functions that satisfy boundary conditions can be used with different levels of modeling accuracy.

Piezoelectric Sensors and Actuators

Here, we assume that the electric field and the elastic field of the piezoelectric actuators and sensors are linearly coupled. Accordingly, the constitutive equations relating mechanical and electrical properties of the smart material take the form

$$D_i=\mathrm{d}\sigma+e^T E_\mathrm{f} \tag{5}$$

$$\varepsilon=S^E\sigma+\mathrm{d}E_\mathrm{f}. \tag{6}$$

Here, σ and ε are the mechanical stress and strain, respectively, E_f and D_i are the electric field and dielectric displacement, respectively, whereas d, S^E, and e^T are the piezoelectric strain/charge coefficient, elastic compliance, and electric permittivity, respectively.

Sensor Equation

Piezoelectric sensors utilize the direct piezoelectric effect. This means that generated stresses within the material generates an electric field, and an accompanying charge distribution. The total charge of the sensor is obtained by integrating the charge density on the patch length.

The electric displacement $D(x,t)$ is expressed as

$$D(x,t)=e_{31}\varepsilon_c(x,t), \tag{7}$$

where e_{31} is the piezoelectric stress/charge constant and $\varepsilon_\mathrm{c}(x,t)$ is the mechanical strain in the piezoelectric sensor.

The total charge on this sensor is obtained by integration of charge distribution, as

$$Q(t)=-b_\mathrm{s}\int_{x_1}^{x_2}q(x,t)\mathrm{d}x=-b_s\left(t_\mathrm{P}+\frac{t_\mathrm{b}}{2}\right)\left(e_{31}\right)\frac{\partial^2 w(x,t)}{\partial x^2}. \tag{8}$$

Here b_s and t_P are the width and thickness of the sensor patch, whereas t_b and $w(x,t)$ are blade thickness and lateral displacement, respectively.

The equation relating input and output of the sensor is given by

$$V^\mathrm{s}(t)=P^T\dot{q}=y(t), \tag{9}$$

where $V^\mathrm{s}(t)$ and $y(t)$ are the sensor voltage, and the output voltage of the system, respectively, and P^T is a constant vector that depends on the sensor material and spanwise position on the blade structure.

Actuator Equation

Piezoelectric actuators utilize the reverse piezoelectric effect. Here, an applied voltage on the actuation patch results in a mechanical strain of both the patch and adjacent structure. The value of this mechanical strain that results from an applied electric field E_f can be written as

$$\varepsilon_\mathrm{A}=d_{31}E_\mathrm{f}=d_{31}\frac{V^\mathrm{a}(t)}{t_\mathrm{a}}, \tag{10}$$

where t_a and $V^\mathrm{a}(t)$ are the piezoelectric patch thickness and actuator input voltage, respectively, and d_{31} is the piezoelectric strain constant.

The resulting mechanical strain results in the following stress in the piezoelectric patch:

$$\sigma_\mathrm{A}=E_\mathrm{P}d_{31}\frac{V^\mathrm{a}(t)}{t_\mathrm{a}}, \tag{11}$$

where E_P is the modulus of elasticity of the piezoelectric material.

Due to its position on side of the structure, wind turbine blade in this case, this stress distribution results in the following applied M_A on the blade beam model

$$M_A = E_P d_{31} z V^a(t), \tag{12}$$

where the moment arm z is calculated as $z = (t_b/2 + t_P)$.

With regards to the controlled response, the expression foe the control force generated by the actuator can be written in the form

$$f_{ctrl} = hV^a(t) = hK_{ctrl}V^s(t), \tag{13}$$

where K_{ctrl} is the controller gain and h is the actuator constant, which varies with actuator type and spanwise position on the blade structure.

Dynamic Equation of a Smart Structure

The governing equation of the smart structure is obtained as

$$M\ddot{q}(t) + Kq(t) = f_{ext} + f_{ctrl}. \tag{14}$$

Here, M and K are the global mass and stiffness matrices, respectively, whereas f_{ext} and f_{ctrl} are the vectors representing external force and actuation control force, respectively.

The governing equation can be transformed into modal coordinates using the relationship

$$q = T\eta, \tag{15}$$

where T is the modal transformation matrix.

Finally, the dynamic equation in generalized coordinates can be obtained by pre-multiplying both sides of the transformed form of Eq. (14) by T^T to get

$$M^*\ddot{q}(t) + K^*q(t) = f^*_{ext} + f^*_{ctrl}. \tag{16}$$

In this equation, M^* and K^* are the generalized mass and stiffness matrices, whereas f^*_{ext} and f^*_{ctrl} are the generalized vectors of external force and actuation force, respectively. The generalized matrices and vectors are given as

$$M^* = T^TMT; K^* = T^TKT; f^*_{ext} = T^Tf_{ext}; f^*_{ctrl} = T^Tf_{ctrl}.$$

Finally, damping in the system is assumed to be proportional, in the form of Rayleigh damping. It is expressed as:

$$C^* = \alpha M^* + \beta K^*, \tag{17}$$

where C^* is the generalized proportional damping matrix, whereas αandβ are the structural damping constants.

Introducing this damping into the smart structure dynamic equation gives

$$M^*\ddot{\eta}(t) + C^*\dot{\eta}(t) + K^*\eta(t) = f^*_{ext} + f^*_{ctrl} \tag{18}$$

$$f^*_{ext} = T^T \mathrm{fr}(t) \tag{19}$$

$$f^*_{ctrl} = T^Tf_{ctrl} = T^Th_iV^a_i(t) = T^Th_iu^a_i(t). \tag{20}$$

Here, $r(t)$ is the external force input (for example impulse disturbance), $u(t)$ is the control input, f is the external force coefficient vector, and h_i is the actuator constant, which varies with actuator type and spanwise position on the blade structure.

State Space Model

The governing equation is written in state space form and is given as

$$\dot{X} = Ax(t) + Bu(t) + Er(t) \tag{21}$$

$$\begin{bmatrix} \dot{x}_1 \\ \dot{x}_1 \\ . \\ . \\ . \\ \dot{x}_n \end{bmatrix} = \begin{bmatrix} 0 & I \\ -M^{*-1}K^* & -M^{*-1}C^* \end{bmatrix}_{n\times n} \begin{bmatrix} x_1 \\ x_1 \\ . \\ . \\ . \\ x_n \end{bmatrix} + \begin{bmatrix} 0 \\ [M^{*-1}T^Th] \end{bmatrix} \begin{Bmatrix} u_1(t) \\ u_2(t) \\ . \\ . \\ u_n(t) \end{Bmatrix} + \begin{bmatrix} 0 \\ [M^{*-1}T^Tf] \end{bmatrix} \begin{Bmatrix} r_1(t) \\ r(t) \\ . \\ . \\ r_n(t) \end{Bmatrix} \tag{22}$$

$$y(t) = Cx(t) + Du(t) \tag{23}$$

$$y(t) = \begin{bmatrix} 0P^T \end{bmatrix} \begin{bmatrix} x_1 \\ x_1 \\ . \\ . \\ . \\ x_n \end{bmatrix}. \tag{24}$$

Here, A, B, C, and D are the system $(n \times n)$ matrix, the control or input $(n \times p)$ matrix, the output $(q \times n)$ matrix, and the transmission $(q \times p)$ matrix, respectively. Also, $x(t), u(t), y(t)$, and $r(t)$ are the state vector, the control input, the system output, and the external force input, respectively.

The size of h and P^T depend on the number of elements used in the modeling as follows:

$$h = E_P d_{31} b\bar{z}[-11..] \tag{25}$$

$$P^T = G_c e_{31} bz[-11..], \tag{26}$$

where E_P and d_{31} are the modulus of elasticity and strain constant of the piezoelectric patch, respectively, whereas b is the width of the piezoelectric patch, $\bar{z} = (t_b + t_P/2)$ is the distance between the beam neutral axis and the piezoelectric patch centerline, G_c is the gain of the signal conditioning device, and e_{31} is the piezoelectric stress/charge constant.

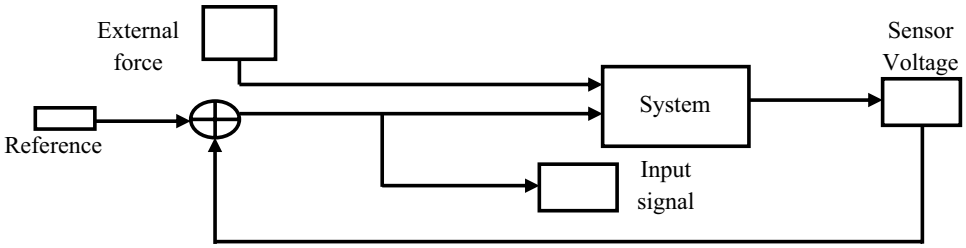

Fig. 3 Simulink block diagram of closed-loop system with adding external force

Controller Design

Several types of controllers can be used to reduce vibrations of wind turbine blades. In an earlier work [13], a PD controller was designed. Here, it is required to design a LQR controller. The control force is applied using piezoelectric patches of different sizes and materials. The LQR performance is defined by:

$$J = \frac{1}{2}\int_0^\infty \left(x^T(t)Qx(t) + u^T(t)Ru(t)\right)\mathrm{d}t, \tag{27}$$

where J is the control objective function, x is the state vector, u is the control input vector, Q and R are the state variables weight matrix, and the control input weight matrix, respectively [16].

The control voltage can be obtained as

$$u = -Gx, \tag{28}$$

where G is the controller gain, calculated from

$$G = R^{-1}B^TP. \tag{29}$$

In Eq. (29), P is the positive definite matrix obtained by solving the algebraic Riccati equation

$$PA + A^TP + Q - PBR^{-1}B^TP = 0. \tag{30}$$

Results

The model described above is validated in [13]. Here, to study the effect of actuator patch size and material, an external aerodynamic force is applied to the smart structure. The shape of the distributed load is assumed to have the cosine distribution $[\cos(\pi x/2L)]$. The external Aerodynamic force (impulse disturbance $r(t)$) is 10 N for duration 40 ms. The Simulink block diagram of closed-loop system is shown in Fig. 3.

The uncontrolled and controlled responses of the system to the disturbing external force are shown in Fig. 4. It is important to examine both controllability and observability of the state space model. Toward this end, it is

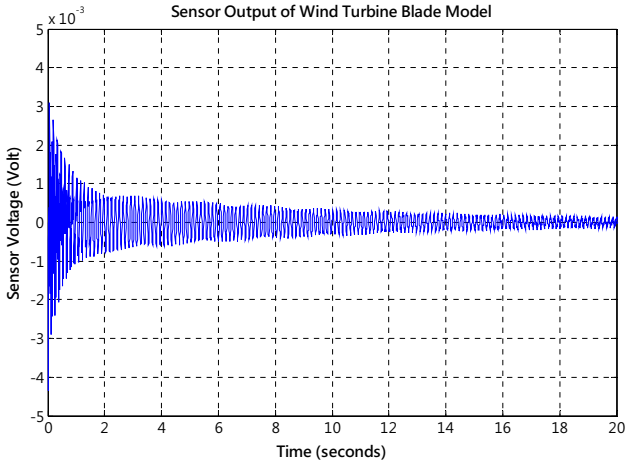

Fig. 4 Closed-loop sensor voltage with no controller of wind turbine blade

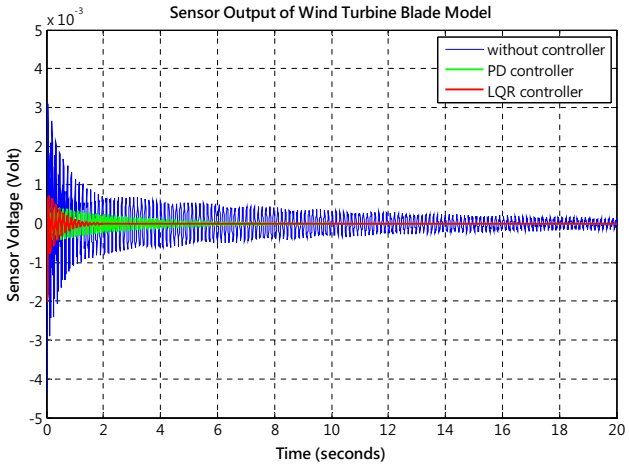

Fig. 5 Comparison of uncontrolled and controlled sensor output of wind turbine blade model

observed that the both the observability matrix and the controllability matrix have the same rank, 4, which is the same as the order of the system. Accordingly, the system is both controllable and observable. Several iterations are used to determine LQR weighting coefficients. Results of

Table 2 Comparison of response characteristics of wind turbine blade model with and without controller

	Without controller	PD controller	LQR controller
Settling time (s)	16.448	2.289	0.674
Peak voltage (V)	0.0043	0.001	0.002
Actuation force (V)		88.48	84.61

this case were obtained using the numerical values of the LQR weighing coefficients: = 250, and$R = 0.001$.

Figure 5 illustrates a comparison between the uncontrolled, PD controlled [13], and LQR controlled response of the system. The considerable improvement achieved using LQR controller over the earlier PD controller is evident. A summary of the numerical values of response parameters for these three cases is presented in Table 2.

Effect of Piezoelectric Size

Dimensions of piezoelectric patches, namely width and thickness, determine the load application capability of these patches, and significantly affect vibration suppression of the smart structure. Using the developed LQR controlled model, the size effect of the piezoelectric actuator is investigated. To study effects of patch width, four values for patch width are used: 0.10, 0.15, 0.20, and 0.25 m, while maintaining a constant patch thickness of ½ mm. Table 3 summarizes the parameters of the closed-loop blade system response for these four cases. To study the effect of patch thickness, four values, with different orders of magnitude, for the thickness are investigated: 0.01, 0.1, 1.0, and 12.0 cm, while maintaining a constant width of 0.107 m. All patch material properties, such as electro-mechanical properties are maintained unchanged. Table 4 lists the parameters of the closed-loop blade system response for these four cases.

Table 5 Electro-mechanical properties of three piezoelectric actuator patch materials

	Density (kg/m^3)	Young's modulus (GPa)	d_{31} (m/V)	e_{31} (C/m^2)
BM500	7650	65	-175×10^{-12}	− 11.9
PSI-5A4E	7800	52	-190×10^{-12}	− 10.56
PSI-5H4E	7800	50	-320×10^{-12}	− 20.37

Results presented in Tables 4 and 5 show the significance of piezoelectric actuator dimensions. As can be seen in Table 4, increasing patch width results in a decrease in actuation force and the maximum displacement. The peak voltage and settling time, however, increase with increasing width. For the specific smart blade system at hand, the optimum width, for minimum maximum displacement, was found to be between 0.1 and 0.2 m. Similarly, Table 5 shows that increasing actuator patch thickness results in decreasing maximum blade displacement, as well as the actuation force. The peak voltage and settling time, however, increase with increasing thickness. Depending on performance function, suitable values may be selected for patch dimensions. For the specific smart blade system at hand, a width between 0.1 and 0.2 m, and thickness between 0.1 and 1 mm produce acceptable results.

Table 3 Comparison of closed-loop smart blade system response parameters at different values of piezoelectric patch width

	Patch 1 (width = 0.1 and thickness = 0.0005)	Patch 2 (width = 0. 15 and thickness = 0.0005)	Patch 3 (width = 0.2 and thickness = 0.0005)	Patch 4 (width = 0.25 and thickness = 0.0005)
Max displacement (m)	0.0017	0.0016	0.0015	0.0014
Peak voltage (V)	0.0019	0.0026	0.0032	0.0037
Actuation force (V)	87.343	64.958	49.874	39.306
Settling time (s)	0.6732	0.7372	0.8605	0.9828

Table 4 Comparison of closed-loop smart blade system response parameters at different values of piezoelectric patch thickness

	Patch 5 (width = 0.107 and thickness = 0.0001)	Patch 6 (width = 0.107 and thickness = 0.001)	Patch 7 (width = 0.107 and thickness = 0.01)	Patch 8 (width = 0.107 and thickness = 0.12)
Max displacement (m)	0.0017	0.0017	0.0016	0.0008
Peak voltage (V)	0.0019	0.0021	0.0034	0.0105
Actuation force (V)	85.505	83.441	63.269	13.83
Settling time (s)	0.6723	0.6752	0.8647	2.101

Table 6 Comparison of closed-loop response parameters for the cases of three different piezoelectric patch materials

	BM500 [17]	PSI-5A4E [18]	PSI-5H4E [18]
Max displacement (m)	0.00159	0.0016	0.0014
Peak voltage (V)	0.0021	0.0019	0.0032
Actuation force (V)	63.179	71.707	45.85
Settling time (S)	0.669	0.664	0.86

Effect of Piezoelectric Material Properties

The electro-mechanical properties of the piezoelectric element of any smart structure have significant impact on the system closed-loop response. Three of the commonly used piezoelectric actuator materials are considered in this study: BM500, PSI-5A4E, and PSI-5H4E. The relevant electro-mechanical coefficients of these materials are listed in Table 5. Table 6 summarizes closed-loop response parameters for the case of piezoelectric patch of width 0.107 m, and thickness of 0.05 cm made of each of these materials.

The above results show that piezoelectric material properties are determining factors in the blade closed-loop response. It clearly shows the dependence of response parameters, such as actuation force, settling time, maximum displacement, and peak voltage, on piezoelectric stress/charge constant (e_{31}). Increasing this coupling constant results in increased values of both the maximum displacement and actuation force. Such increase, however, results also in decreased values of both peak voltage and closed-loop settling time.

Conclusions

In this work, a simulation is carried out to facilitate studying the size and material effects of a piezoelectric actuator and sensor on the dynamic response of a wind turbine blade. Results demonstrated the ability of approximate analytical methods to deal effectively with various blade cross sections. PD and LQR controllers are designed to determine the amount of actuation force required on the smart system. The simulation results show that LQR controller produces considerable reduction in both the settling time and the actuation force. Results also show that increasing the width or thickness of piezoelectric actuator results in a decrease of the maximum displacement and actuation force and an increase of peak voltage and settling time. Three types of piezoelectric actuator materials are considered. Investigation results shows that using a material with higher piezoelectric stress/charge constant (decrease in absolute value of negative e_{31}) increases both maximum displacement and actuation force. This also has the effect of reducing the peak voltage and settling time.

References

1. Achawakorn K, Jearsiripongkul T (2012) Vibration analysis of exponential cross-section beam using Galerkin's method. Int J Appl Sci Technol 2(6):7–13
2. Bazoune A, Khulief YA (1992) A finite beam element for vibration analysis of rotating tapered timoshenko beams. J Sound Vib 156(1):141–164
3. Kumar GVR, Sujatha C (2010) Forced vibration analysis of wind turbine rotor. Adv Vib Eng 9(3):285–296
4. Crawley EF, De Luis J (1987) Use of piezoelectric actuators as elements of intelligent structures. AIAA J 25(10):1373–1385
5. Han J, Rew K, Lee I (1997) An experimental study of active vibration control of composite structures with a piezo-ceramic actuator and a piezo-film sensor. Smart Mater Struct 6(5):549–558
6. Zhang J, He L, Wang E, Gao R (2008) A LQR controller design for active vibration control of flexible structures. In: Proceedings of the 2008 IEEE Pacific-Asia workshop on computational intelligence and industrial application, vol 01, pp 127–132
7. Zhang J, He L, Wang E, Gao R (2009) Active vibration control of flexible structures using piezoelectric materials. In: Proceedings of the 2009 international conference on advanced computer control, pp 540–545
8. Manjunath TC, Bandyopadhyay B (2006) Smart control of cantilever structures using output feedback. Int J Sim Syst Sci Technol 7(4–5):51–68
9. Manjunath TC, Bandyopadhyay B (2004) Vibration control of a smart structure using periodic output feedback technique. Asian J Control 6(1):74–87
10. Roy T, Chakraborty D (2009) Genetic algorithm based optimal control of smart composite shell structures under mechanical loading and thermal gradient. Smart Mater Struct 18(11):115006 (12 pp)
11. Kumar A, Chhabra D (2013) Design of neural network controller for active vibration control of cantilever plate with piezo-patch as sensor/actuator. Int J Modern Eng Res 3(4):2481–2488
12. Zoric ND, Simonovic AM, Mitrovic ZS, Stupar SN (2012) Optimal vibration control of smart composite beams with optimal size and location of piezoelectric sensing and actuation. J Intell Mater Syst Struct 24(4):499–526
13. Abdelmaksoud SI (2014) Optimal active vibration suppression of smart composite wind turbine blades. Master thesis, King Fahd University of Petroleum and Minerals, Dhahran, Saudi Arabia
14. Manwell JF, McGowan JG, Rogers AL (2009) Wind energy explained: theory, design and application. Wiley, UK
15. Ladson CL, Center LR (1996) Computer program to obtain ordinates for NACA airfoils. National Aeronautics and Space Administration, Langley Research Center
16. Li Y, Liu J, Wang Y (2008) Design approach of weighting matrices for LQR based on multi-objective evolution algorithm. In: 2008 international conference on information and automation, vol. 2, pp 1188–1192
17. Sensortech.ca (2014) Acoustic transducers, composites, hydrophones, echo sounders & piezoelectric ceramics by Sensor Technology Ltd.', 2014. [Online]. http://www.sensortech.ca/site/index.cfm. Accessed 10 May 2015
18. Piezo.com (2014) Piezoceramic materials & properties 2014. [Online]. http://www.piezo.com/prodmaterialprop.html. Accessed 10 May 2015